Finite element vibration analysis of laminated composite folded plate structures

A. Guha Niyogi, M.K. Laha and P.K. Sinha *
Department of Aerospace Engineering, Indian Institute of Technology, Kharagpur – 721 302, India

Received 4 April 1999
Revised 22 October 1999

A nine-noded Lagrangian plate bending finite element that incorporates first-order transverse shear deformation and rotary inertia is used to predict the free and forced vibration response of laminated composite folded plate structures. A 6×6 transformation matrix is derived to transform the system element matrices before assembly. The usual five degrees-of-freedom per node is appended with an additional drilling degree of freedom in order to fit the transformation. The present finite element results show good agreement with the available semi-analytical solutions and finite element results. Parametric studies are conducted for free and forced vibration analysis for laminated folded plates, with reference to crank angle, fibre angle and stacking sequence. The natural frequencies and mode shapes, and forced vibration responses furnished here may serve as a benchmark for future investigations.

Keywords: Composite, finite element method, stacking sequence, transverse shear, folded plates, crank angle, transformation

1. Introduction

Folded plate structures have a wide range of engineering applications in aircraft fuselages, ship hulls, buildings, bridges and vehicle chassis, among other structures. With the advent of fiber-reinforced laminated composites, the applicability of folded plate structures has increased many folds due to their low weight, high stiffness and high strength properties. Structural properties of the laminated composites can be tailored to realize better performance by controlling the lamination angle and stacking sequence. Literature in the field of dynamic analysis of laminated composite folded plates is scanty and the present paper is meant to address the dynamic behaviour of composite folded plate structures, in view of its tremendous potentials.

Historically, Goldberg and Leve [8] pioneered the exact static analysis of folded plate structures. Irie et al. [10] calculated the natural frequencies of cantilever folded plates by Ritz method. Ohga and Shinematsu [17] applied boundary element-transfer matrix method to solve the bending problem of folded plates. Golley and Grice [9] and Eterovic and Godoy [7] employed finite strip methods. Danial [4] and Danial et al. [5] introduced a concept entitled Spectral Element Method. Liu and Huang [12] had used a finite element-transfer matrix method to analyze one- and two-fold folded plates. Bathe [1] and Zienkeiwicz and Taylor [21] had presented a method of flat shell analysis, which can be directly applied to folded plate structures. However, all these works relate to isotropic folded plate structures only.

For the finite element analysis of laminated composite plates with first and higher order shear deformation theories (FST, HST) several works may be referred to. The works of Reddy [18], Kant et al. [11], Meimaris and Day [16], Bert and Chen [2], Chatterjee and Kulkarni [3], Dong and Chun [6] and Maiti and Sinha [13–15] may be cited to name only a few. Recently, Suresh and Malhotra [19] conducted damped free vibration analysis of composite box beams using 4 noded plate finite element with five degrees of freedom (u, v, w, θ_x and θ_y) per node.

In the present analysis the FST is adopted to analyze the laminated composite folded plates. A shear correction factor of $5/6$ has been assumed, which is derived from the Timoshenko beam concept by applying the energy principle. A comparative study using FST and HST [13–15] clearly indicates that the present first order shear deformation theory provides excellent results for moderately thick composite beams, plates and shells for all practical situations. Attention is therefore restricted to application of FST for the development

*Corresponding author. Tel.: +91 3222 77997; Fax: +91 3222 55303/55239; E-mail: pksinha@aero.iitkgp.ernet.in

Shock and Vibration 6 (1999) 273–283
ISSN 1070-9622 / $8.00

of the finite element analysis procedure for composite folded plates.

The transformations used to generate the global mass, stiffness and load arrays are presented. The results of free vibration analysis and also transient analysis of cantilever laminated folded plates, subjected to suddenly applied step loading are presented. The transient analysis is done using the Newmark's direct integration scheme [1]. Parametric studies are conducted by varying the crank angle, fibre orientation and number of layers for the laminated composite folded plate. The present methodology can easily be applied to the analysis of box beams and closed structures.

2. Theoretical formulation

In the classical thin plate theory, it is assumed that normals to the mid-plane before deformation remain normal and plane after deformation. This assumption neglects the effect of transverse shear deformation. Here Mindlin's assumptions, as given below, are adopted to incorporate the first order transverse shear effects:

i) The deflection of the mid-plane of the plate is small compared to the plate thickness.
ii) The transverse normal stress is neglected.
iii) Normals to the mid-plane of the plates before deformation remain straight but not necessarily normal after deformation.

The displacements of the plate are fully described by five components: $u, v, w, \theta_x, \theta_y$, where u, v and w are displacements along the x, y and z-directions and θ_x and θ_y are rotations about y- and x-axes. The positive sign conventions for displacements and stress resultants are illustrated in Fig. 1.

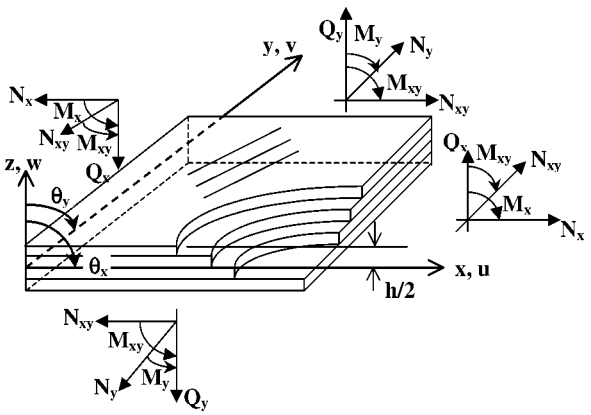

Fig. 1. The laminated composite plate with positive displacements, rotations and stress resultants.

2.1. Flat plate finite element formulation for composite plates

The displacements at a node j of a plate element are $u_j, v_j, w_j, \theta_{xj}$ and θ_{yj}. The displacements at any point within the element can be expressed as

$$\begin{Bmatrix} u \\ v \\ w \\ \theta_x \\ \theta_y \end{Bmatrix} = \sum_{j=1}^{9} N_j [I_5] \begin{Bmatrix} u_j \\ v_j \\ w_j \\ \theta_{xj} \\ \theta_{yj} \end{Bmatrix}, \tag{1}$$

where $[I_5]$ is a 5×5 identity matrix and N_j are Lagrangian interpolation functions [1]. For Mindlin plates the following relationship is valid:

$$\begin{Bmatrix} u \\ v \\ w \end{Bmatrix} = \begin{Bmatrix} u_0 + z\theta_x \\ v_0 + z\theta_y \\ w_0 \end{Bmatrix} \quad \text{and}$$

$$\begin{Bmatrix} \theta_x \\ \theta_y \end{Bmatrix} = \begin{Bmatrix} \dfrac{\partial w}{\partial x} + \phi_x \\ \dfrac{\partial w}{\partial y} + \phi_y \end{Bmatrix}, \tag{2}$$

where θ_x and θ_y are the total rotations, ϕ_x and ϕ_y are the average shear deformations about the y and x axes, and u_0, v_0 and w_0 are the mid-plane translations along x, y and z directions.

2.2. Stiffness matrix of plate element

The stiffness matrix of the plate element assumes the form

$$[K]_e = \int_{A_e} [B]^{\mathrm{T}} [D][B] \, \mathrm{d}A, \tag{3}$$

where

$$\{\varepsilon\} = [B]\{\delta\}. \tag{4}$$

Here, $\{\varepsilon\}$ is the strain vector and $\{\delta\}$ is the nodal displacement vector. The strain–displacement matrix $[B]$ is given in

$$[B]\{\delta\} = \sum_{j=1}^{9} \begin{bmatrix} N_{j,x} & 0 & 0 & 0 & 0 \\ 0 & N_{j,y} & 0 & 0 & 0 \\ N_{j,y} & N_{j,x} & 0 & 0 & 0 \\ 0 & 0 & 0 & N_{j,x} & 0 \\ 0 & 0 & 0 & 0 & N_{j,y} \\ 0 & 0 & 0 & N_{j,y} & N_{j,x} \\ 0 & 0 & N_{j,y} & 0 & N_j \\ 0 & 0 & N_{j,x} & N_j & 0 \end{bmatrix} \begin{Bmatrix} u_{0j} \\ v_{0j} \\ w_{0j} \\ \theta_{xj} \\ \theta_{yj} \end{Bmatrix}. \tag{5}$$

$[D]$ is the stiffness matrix given by

$$[D] = \begin{bmatrix} A_{11} & A_{12} & A_{16} & B_{11} & B_{12} & B_{16} & 0 & 0 \\ A_{12} & A_{22} & A_{26} & B_{12} & B_{22} & B_{26} & 0 & 0 \\ A_{16} & A_{26} & A_{66} & B_{16} & B_{26} & B_{66} & 0 & 0 \\ B_{11} & B_{12} & B_{16} & D_{11} & D_{12} & D_{16} & 0 & 0 \\ B_{12} & B_{22} & B_{26} & D_{12} & D_{22} & D_{26} & 0 & 0 \\ B_{16} & B_{26} & B_{66} & D_{16} & D_{26} & D_{66} & 0 & 0 \\ 0 & 0 & 0 & 0 & 0 & 0 & A_{44} & A_{45} \\ 0 & 0 & 0 & 0 & 0 & 0 & A_{45} & A_{55} \end{bmatrix} \quad (6)$$

where

$$A_{ij}, B_{ij}, D_{ij} = \sum_{k=1}^{N} \int_{z_{k-1}}^{z_k} \left(Q_{ij}\right)^k (1, z, z^2)\,\mathrm{d}z, \quad i, j = 1, 2, 6 \quad (7a)$$

and

$$A_{ij} = \sum_{k=1}^{N} \int_{z_{k-1}}^{z_k} \kappa (Q_{ij})^k\,\mathrm{d}z, \quad i, j = 4, 5,\ \kappa = 5/6. \quad (7b)$$

Here, Q_{ij} are the elements of off-axis stress–strain relations. Q_{ij}^k relates stresses and strains in the kth layer by the relation $\sigma_i^k = Q_{ij}^k \varepsilon_j^k$, $i, j = 1, 2, 6$, whereas $\sigma_l^k = Q_{lm}^k \varepsilon_m^k$, $l, m = 4, 5$ and κ is the shear correction factor. Q_{ij}^k for the kth layer is expressed as

$$\begin{Bmatrix} \sigma_1 \\ \sigma_2 \\ \sigma_6 \end{Bmatrix}^k = \begin{bmatrix} Q_{11} & Q_{12} & Q_{16} \\ Q_{12} & Q_{22} & Q_{26} \\ Q_{16} & Q_{26} & Q_{66} \end{bmatrix}^k \begin{Bmatrix} \varepsilon_1 \\ \varepsilon_2 \\ \varepsilon_6 \end{Bmatrix}^k \quad \text{and}$$

$$\begin{Bmatrix} \sigma_4 \\ \sigma_5 \end{Bmatrix}^k = \begin{bmatrix} Q_{44} & Q_{45} \\ Q_{45} & Q_{55} \end{bmatrix}^k \begin{Bmatrix} \varepsilon_4 \\ \varepsilon_5 \end{Bmatrix}^k. \quad (8)$$

Here, $\sigma_1, \sigma_2, \sigma_4, \sigma_5$, and σ_6 denote $\sigma_x, \sigma_y, \tau_{yz}, \tau_{zx}$ and τ_{xy}, respectively, and $\varepsilon_1, \varepsilon_2, \varepsilon_4, \varepsilon_5$, and ε_6 stands for $\varepsilon_x, \varepsilon_y, \gamma_{yz}, \gamma_{zx}$ and γ_{xy}, respectively.

2.3. Mass matrix of plate element

In matrix form the equation of motions for the Mindlin plate may be written as follows:

$$\begin{Bmatrix} N_{x,x} + N_{xy,y} \\ N_{xy,x} + N_{y,y} \\ Q_{x,x} + Q_{y,y} + q \\ M_{x,x} + M_{xy,y} \\ M_{xy,x} + M_{y,y} \end{Bmatrix} = \begin{bmatrix} I & 0 & 0 & P & 0 \\ 0 & I & 0 & 0 & P \\ 0 & 0 & I & 0 & 0 \\ P & 0 & 0 & Q & 0 \\ 0 & P & 0 & 0 & Q \end{bmatrix} \begin{Bmatrix} \ddot{u}_0 \\ \ddot{v}_0 \\ \ddot{w}_0 \\ \ddot{\theta}_x \\ \ddot{\theta}_y \end{Bmatrix},$$

$$(I, P, Q) = \int_{-h/2}^{h/2} \rho\left(1, z, z^2\right)\,\mathrm{d}z$$

or

$$\{F\} = [\rho]\{A\}, \quad (9)$$

where $\{F\}$ is the force vector, $[\rho]$ is the inertia matrix, and $\{A\}$ is the acceleration vector. The mass matrix of the plate element is given by

$$[M]_e = \int_{A_e} [N]^{\mathrm{T}} [\rho] [N]\,\mathrm{d}A, \quad (10)$$

where $[N]$ are the Lagrangian interpolation functions.

2.4. Load vector

The element load vector for forced vibration analysis is given by

$$\int_{A_e} [N]^{\mathrm{T}} q\,\mathrm{d}A, \quad (11)$$

where q is the transverse load intensity on the element. The integration in every case is carried out over the area of the plate element. Generally, a 3-point Gauss quadrature is adopted to compute the bending stiffness of the elements, whereas a 2-point integration is adopted to calculate the shear stiffness, mass matrix, and element force vector. A 2-point eliminates the shear locking in thin plates. It is also known that a 2-point integration for both the mass matrix and force vector is adequate.

2.5. Transformations for folded plate

With reference to Fig. 2, the relations between local and global displacements are given as

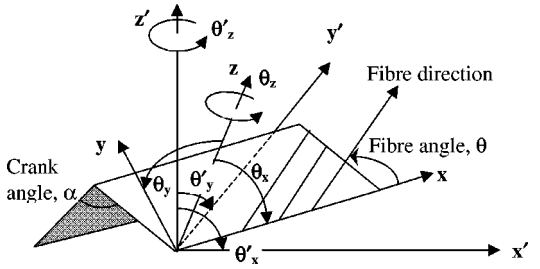

Fig. 2. Local (unprimed) and global (primed) axes system for a typical folded plate element. The least angle contained between positive x' and x axes is denoted as (x', x).

$$\begin{Bmatrix} u \\ v \\ w \\ \theta_x \\ \theta_y \\ \theta_z \end{Bmatrix} = \begin{bmatrix} \cos(x',x) & \cos(y',x) & \cos(z',x) \\ \cos(x',y) & \cos(y',y) & \cos(z',y) \\ \cos(x',z) & \cos(y',z) & \cos(z',z) \\ 0 & 0 & 0 \\ 0 & 0 & 0 \\ 0 & 0 & 0 \end{bmatrix}$$

$$\begin{bmatrix} 0 & 0 & 0 \\ 0 & 0 & 0 \\ 0 & 0 & 0 \\ \cos(y',y) & -\cos(x',y) & \cos(z',y) \\ -\cos(y',x) & \cos(x',x) & -\cos(z',x) \\ \cos(y',z) & -\cos(x',z) & \cos(z',z) \end{bmatrix} \begin{Bmatrix} u' \\ v' \\ w' \\ \theta'_x \\ \theta'_y \\ \theta'_z \end{Bmatrix}$$

or

$$\{u\} = [T]\{u'\}. \tag{12}$$

Finally, the global stiffness, mass matrices and force vector are expressed as

$$[K']_e = [T]^{\mathrm{T}}[K]_e[T], \tag{13}$$

$$[M']_e = [T]^{\mathrm{T}}[M]_e[T], \tag{14}$$

$$\{f'\}_e = [T]^{\mathrm{T}}\{f\}_e. \tag{15}$$

However, before applying the transformation, the 45×45 stiffness and mass matrices is blown up to 54×54 size, to accommodate the nine θ_z drilling degrees of freedom per element. The off-diagonal terms corresponding to the θ_z terms are set to zero, while a very small positive number is introduced at the corresponding leading diagonal terms. This small number is taken to be 1000 times smaller than the smallest leading diagonal term of the corresponding element matrix before blowing up [1]. The load vector is similarly enlarged by incorporating null terms in the θ_z positions.

The free vibration analysis involves the solution of

$$[M']\{\ddot{x}'\} + [K']\{x'\} = \{0\} \tag{16}$$

and, the method of subspace iteration [1] is adopted to extract the eigenpairs. In the forced vibration analysis, the damping is neglected, and the force term replaces the null vector in the right hand side of Eq. (16). Newmark's explicit integration technique [1] is adopted for the transient analysis.

3. Numerical results and discussion

The finite element formulation described in the earlier section has been used to compare the present results with the published ones and also to generate numerical results to study the effects of crank angle, fibre angle and number of plies used, on the non-dimensional frequencies and responses of composite folded plates. The definitions for non-dimensionalised frequencies are given along with Tables 1 and 2.

Example 1. The results of free vibration analysis of isotropic single-fold and double-fold cantilever folded plates (Fig. 3) are presented in Table 1 and compared with those of Liu et al. [12] and Irie et al. [10]. The geometry of the folded plates is defined in Fig. 3. Here elastic modulus E, Poisson's ratio ν, and density ρ are taken as 10.92×10^9 N/m^2, 0.30, and 1000 kg/m^3, respectively. The length of the cantilever is taken as 1.5 m for single fold folded plates and 2.0 m for two-fold folded plates. The present analysis is carried out with multiple layers of isotropic material. The results are found to be in good agreement with previous works on isotropic folded plates.

Example 2. Free vibration analysis of single-fold cantilever folded plates with E-glass–Epoxy composite has been carried out for the geometries shown in Fig. 3, and the results of the parametric studies are presented in Tables 2, 3, and 4. The data used are $E_1 = 60.7 \times 10^9$ N/m^2, $E_2 = 24.8 \times 10^9$ N/m^2, $G_{12} = G_{13} = G_{23} = 12.0 \times 10^9$ N/m^2, $\nu_{12} = \nu_{21} = 0.23$, $\rho = 1300$ kg/m^3, and 4×3 mesh. In Table 2, results are provided for the stacking sequences of the type $[\theta/-\theta/\theta]$, where θ varies from 0° to 60°. It is observed that the fundamental frequency decreases steadily with increasing fibre angle, the overall depth remaining unchanged. As shown in Fig. 4, for the single folded composite plates with crank angles 150° and 90°, and for fibre orientations 30°/−30° and 45°/−45°, respectively, the first and third modes are found to be torsion modes, while the second mode is a symmetric

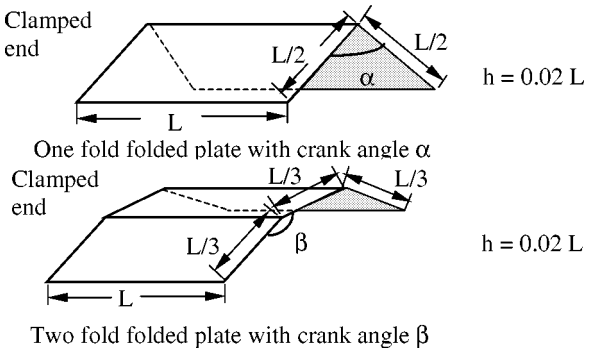

Fig. 3. Geometry of the folded plate used in examples 1, 2, 4, 5 and 6.

Table 1
Results of free vibration analysis of isotropic folded plate

Description of the folded plate	Mode number	Mesh size	λ_i		
			Present case	Liu et al. [12]	Irie et al. [10]
1-fold folded plate,	1	4×2	0.049	0.0491	0.0492
$\alpha = 90^\circ$	2		0.0971	0.0971	0.0977
	3		0.1881	0.1786	0.1794
	4		0.2183	0.2084	0.2101
	5		0.3505	0.3558	0.3573
1-fold folded plate,	1	4×3	0.049	0.0491	0.0492
$\alpha = 120^\circ$	2		0.0941	0.0943	0.0949
	3		0.1883	0.1787	0.1795
	4		0.216	0.2065	0.2082
	5		0.293	0.2971	0.2984
1-fold folded plate,	1	4×2	0.0491	0.0491	0.0492
$\alpha = 150^\circ$	2		0.0804	0.0812	0.0816
	3		0.1883	0.1787	0.1795
	4		0.1942	0.1912	0.1927
	5		0.2256	0.2210	0.2227
Flat plate,	1	4×4	0.0200	0.0200	0.0201
$\alpha = 180^\circ$	2		0.0489	0.0492	0.0493
	3		0.1230	0.1235	0.1234
	4		0.1567	0.1566	0.1577
	5		0.1784	0.1787	0.1796
2-fold folded plate,	1	3×2	0.1249	0.1249	–
$\beta = 90^\circ$	2		0.1252	0.1260	
	3		0.2697	0.2579	
	4		0.2830	0.2892	
	5		0.3266	0.3286	
2-fold folded plate,	1	3×2	0.0971	0.1000	–
$\beta = 120^\circ$	2		0.1239	0.1241	
	3		0.2578	0.2571	
	4		0.2691	0.2630	
	5		0.2906	0.2986	
2-fold folded plate,	1	6×3	0.0679	0.0687	–
$\beta = 150^\circ$	2		0.1142	0.1145	
	3		0.2065	0.2100	
	4		0.2410	0.2415	
	5		0.2573	0.2571	

Note: $\lambda_i = \omega_i L\sqrt{\rho(1-v^2)/E}$.

bending mode. It may be noted that the ridgeline remains nearly undeformed for these modes and is instrumental in imparting additional stiffness compared to flat plates. This, in turn, has resulted in higher non-dimensional fundamental frequencies to folded plates compared to flat plate, as seen in Table 2.

Table 3 provides natural frequencies for 4-layered symmetric and anti-symmetric angle-ply and cross ply laminates. Here it is observed that anti-symmetric angle-ply with lower values of fibre angle produces higher fundamental frequency. It may also be noted from Table 4 that the fundamental frequencies have an

Table 2
Non-dimensional natural frequencies for single fold composite cantilever folded plates

Crank angle α	λ_i	Stacking sequence $[\theta/-\theta/\theta]$			
		$\theta = 0°$	$\theta = 30°$	$\theta = 45°$	$\theta = 60°$
90°	1	0.0391	0.0390	0.0381	0.0367
	2	0.0675	0.0712	0.0753	0.0804
	3	0.1556	0.1473	0.1406	0.1399
120°	1	0.0391	0.0390	0.0381	0.0366
	2	0.0664	0.0697	0.0731	0.0768
	3	0.1557	0.1472	0.1404	0.1331
150°	1	0.0391	0.0389	0.0380	0.0366
	2	0.0609	0.0624	0.0629	0.0624
	3	0.1557	0.1455	0.1377	0.1306
180°	1	0.0201	0.0177	0.0158	0.0141
	2	0.0392	0.0387	0.0378	0.0364
	3	0.1015	0.1015	0.0948	0.0862

Note: $\lambda_i = \omega_i L\sqrt{\rho(1-v_{12}^2)/E_1}$.

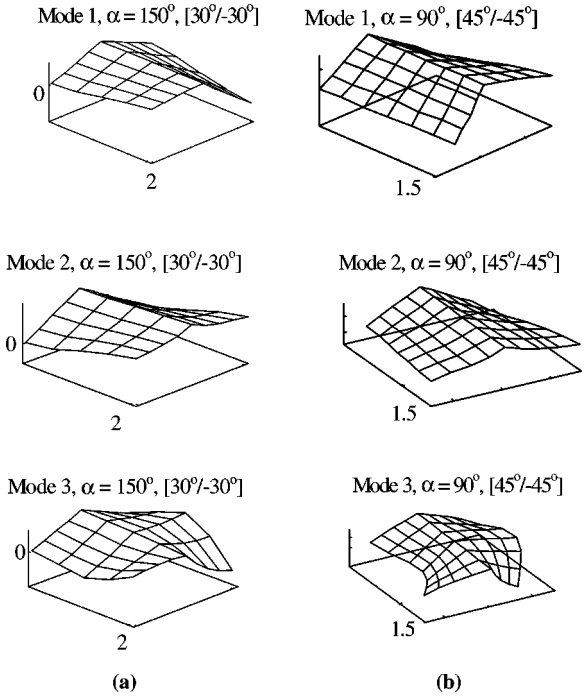

Fig. 4. First, second and third mode shapes of E-glass–Epoxy cantilever composite single fold folded plate with (a) crank angle $\alpha = 150°$, ply arrangement $30°/-30°$, and (b) crank angle $\alpha = 90°$, ply arrangement $45°/-45°$.

increasing trend with the increase in the number of layers, while the fibre angles and thickness are kept invariant. Anti-symmetric plies have shown higher fundamental frequencies.

Tables 5, 6 and 7 represent the first three natural frequencies for two-fold folded plates (refer Fig. 3). 6×3 mesh are used. For $\beta = 120°$, the mode shapes of a two-fold composite folded plate are shown in Fig. 5(b). The first mode is a torsion mode. The second mode is a symmetric bending mode and the third is a symmetric mode too, though complex in shape. However this trend is not repeated for $\beta = 90°$, as shown in Fig. 5(a). Thus, Fig. 5 shows that the mode shapes for two-fold folded plates depend on the crank angles β heavily, as also on the fibre angles. This is unlike single fold folded plates, where only fibre angles and number of plies are of importance, and the values of first and the third frequencies are nearly invariant for a given fibre angle and number of plies irrespective of the crank angle α. From Table 5 it is observed that for the type $[\theta/-\theta/\theta]$, there is a decreasing trend of first frequencies with increase in the value of θ, but the case of 2-fold plate with a crank of 90° now shows a reverse trend. It may also be noted that for isotropic and composite single-fold plates and two-fold isotropic folded plates the first frequency is found to remain practically unchanged for same material properties and fibre angles (refer Tables 1, 2, 3, and 4, and [10,12]). This is also not generally true for 2-fold composite folded plates and the crank angle is seen to affect the fundamental frequencies considerably. From Table 6 it is seen that anti-symmetric plies produce higher fundamental frequencies. Table 7 reveals that an increase in number of layers increases the fundamental frequencies. It may also be noted here that for

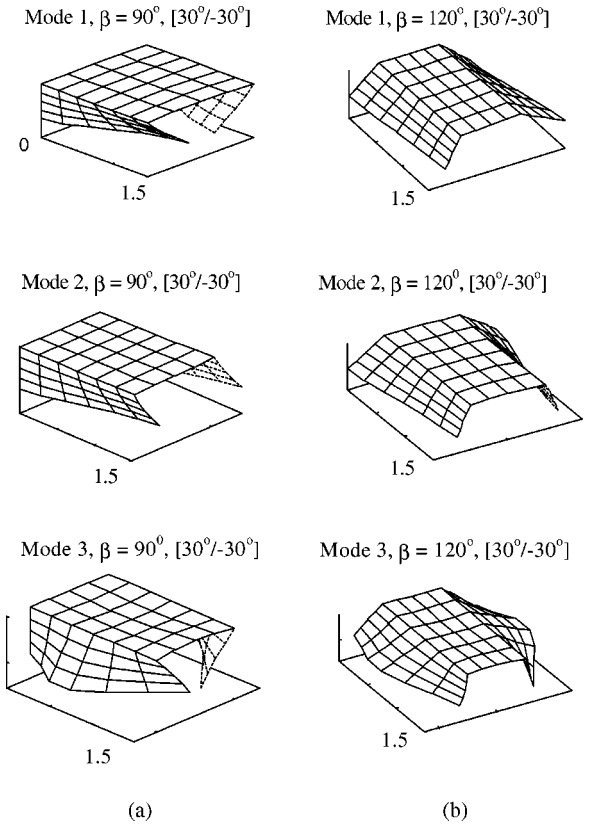

Fig. 5. First, second and third mode shapes of E-glass–Epoxy composite twofold folded plate with (a) crank angle $\beta = 90°$, ply arrangement $30°/-30°$, and (b) crank angle $\beta = 120°$, ply arrangement $30°/-30°$.

single-fold folded plates the $[30°/-30°]_3$ laminations produce highest fundamental frequencies whereas the $0°$ or $(0°/90°)_2$ lamination produce the highest fundamental frequencies for two-fold folded plates. Finally, Table 8 shows a comparative study of results obtained by applying 2-point and 3-point integration for mass matrices. The table reveals that there is no perceptible difference of results, and a 2-point integration may be employed for computational efficiency.

Example 3. To check the accuracy of the code developed for forced vibration, the central deflection of a square, clamped, cross-ply laminate has been obtained using this code. The data used are $L = 25$ cm, $h = 5$ cm, $E_1/E_2 = 25$, $E_2 = 2.1 \times 10^6$ N/cm^2, $\nu_{12} = \nu_{21} = 0.25$, $G_{12} = G_{13} = G_{23} = 0.5\ E_2$, $\rho = 8.0 \times 10^6$ N s^2/cm^4. A 4×4 mesh is used. The central deflection due to a suddenly applied step loading $q = 10$ N/cm^2, that is imposed at time $t = 0$ and is not withdrawn, is presented in Fig. 6. Damping

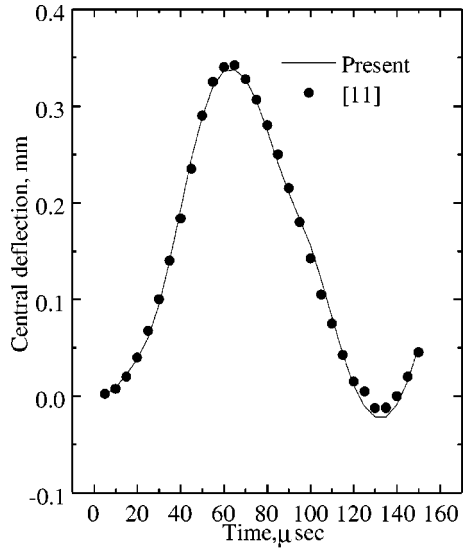

Fig. 6. Central deflection versus time for a $0°/90°/0°$ square clamped laminated plate with suddenly applied pulse loading (4×4 mesh).

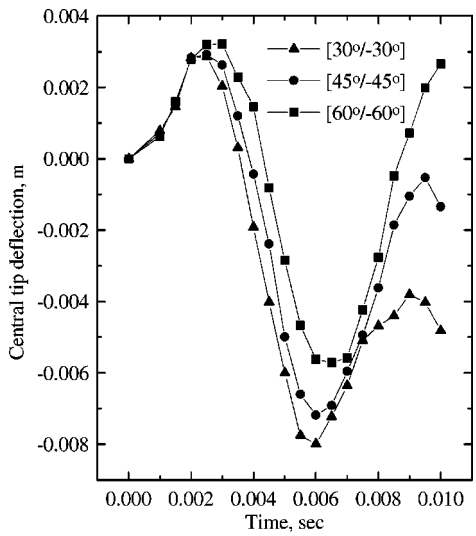

Fig. 7. Comparative central tip deflection versus time for 2-fold E-glass–Epoxy 2 layered folded plate with crank angle $\beta = 120°$ for various fibre angles (ref. Fig. 3) with $L = 1.5$ m and suddenly applied step load $q = 1.0 \times 10^5$ N/m^2.

has not been accounted in this analysis. The time step for the explicit integration scheme is taken as 5 microseconds. The results conform satisfactorily to those of Kant [11].

Example 4. The comparative study of mid-point tip deflection of two-fold cantilever folded plate (Fig. 3) with crank angle, $\beta = 120°$ is applied for two ply

Table 3
Non-dimensional natural frequencies for two-fold composite cantilever folded plates

Crank angle α	λ_i	Stacking sequence			
		$[30^\circ/-30^\circ]_S$	$[30^\circ/-30^\circ]_2$	$[0^\circ/90^\circ]_S$	$[0^\circ/90^\circ]_2$
90°	1	0.0394	0.0397	0.0387	0.0369
	2	0.0719	0.0724	0.0704	0.0774
	3	0.1488	0.1496	0.1525	0.1397
120°	1	0.0394	0.0398	0.0387	0.0369
	2	0.0703	0.0707	0.0688	0.0750
	3	0.1488	0.1497	0.1526	0.1399
150°	1	0.0394	0.0398	0.0386	0.0370
	2	0.0627	0.0629	0.0611	0.0642
	3	0.1475	0.1497	0.1509	0.1400

Table 4
Non-dimensional natural frequencies for two-fold composite cantilever folded plates

Crank angle α	λ_i	Stacking sequence				
		$[30^\circ/-30^\circ]$	$[30^\circ/-30^\circ]_S$	$[30^\circ/-30^\circ]_2$	$[30^\circ/-30^\circ/30^\circ]_S$	$[30^\circ/-30^\circ]_3$
90°	1	0.0381	0.0394	0.0397	0.0399	0.0400
	2	0.0701	0.0719	0.0724	0.0726	0.0728
	3	0.1443	0.1488	0.1496	0.1503	0.1506
120°	1	0.0381	0.0394	0.0398	0.0399	0.0401
	2	0.0686	0.0703	0.0707	0.0710	0.0711
	3	0.1444	0.1488	0.1497	0.1504	0.1507
150°	1	0.0381	0.0394	0.0398	0.0399	0.0401
	2	0.0614	0.0627	0.0629	0.0631	0.0632
	3	0.1443	0.1475	0.1497	0.1497	0.1507

Table 5
Non-dimensional natural frequencies for two-fold composite cantilever folded plates

Crank angle β	λ_i	Stacking sequence $[\theta/-\theta/\theta]$			
		$\theta = 0^\circ$	$\theta = 30^\circ$	$\theta = 45^\circ$	$\theta = 60^\circ$
90°	1	0.0844	0.0887	0.0914	0.0924
	2	0.0937	0.0992	0.1035	0.1081
	3	0.2049	0.2008	0.1988	0.1970
120°	1	0.0796	0.0771	0.0745	0.0712
	2	0.0851	0.0930	0.0993	0.1057
	3	0.2047	0.1994	0.1970	0.1950
150°	1	0.0567	0.0546	0.0519	0.0491
	2	0.0817	0.0864	0.0898	0.0914
	3	0.1765	0.1698	0.1620	0.1561

composites with different fibre angles. Data used are $E_1 = 60.7 \times 10^9$ N/m^2, $E_2 = 24.8 \times 10^9$ N/m^2, $G_{12} = G_{13} = G_{23} = 12.0 \times 10^9$ N/m^2, $\nu_{12} = \nu_{21} = 0.23$, $\rho = 1300$ kg/m^3, $q = 1.0 \times 10^5$ N/m^2. The load is again a step type load, initiating at $t = 0$ and not withdrawn. The results are plotted in Fig. 7. A time step of 5 and 10 μs has produced same responses. Here the guideline of Tsui and Tong [20] has been followed to fix the

Table 6
Non-dimensional natural frequencies for single fold composite cantilever folded plates

Crank angle β	λ_i	Stacking sequence			
		$[30°/-30°]_S$	$[30°/-30°]_2$	$[0°/90°]_S$	$[0°/90°]_2$
90°	1	0.0901	0.0924	0.0896	0.0987
	2	0.0989	0.0969	0.0934	0.0993
	3	0.2035	0.2072	0.2044	0.1992
120°	1	0.0781	0.0792	0.0761	0.0772
	2	0.0931	0.0920	0.0893	0.0987
	3	0.2029	0.2068	0.2041	0.1993
150°	1	0.0551	0.0555	0.0533	0.0522
	2	0.0869	0.0867	0.0840	0.0906
	3	0.1703	0.1700	0.1628	0.1670

Table 7
Non-dimensional natural frequencies for single fold composite cantilever folded plates

Crank angle β	λ_i	Stacking sequence				
		$[30°/-30°/30°]$	$[30°/-30°]_S$	$[30°/-30°]_2$	$[30°/-30°/30°]_S$	$[30°/-30°]_3$
90°	1	0.0887	0.0901	0.0924	0.0918	0.0930
	2	0.0992	0.0989	0.0969	0.0983	0.0973
	3	0.2008	0.2035	0.2072	0.2074	0.2086
120°	1	0.0771	0.0781	0.0792	0.0790	0.0795
	2	0.0930	0.0931	0.0920	0.0930	0.0926
	3	0.1994	0.2029	0.2068	0.2065	0.2082
150°	1	0.0546	0.0551	0.0555	0.0555	0.0558
	2	0.0864	0.0869	0.0867	0.0871	0.0871
	3	0.1698	0.1703	0.1700	0.1700	0.1704

Table 8
Non-dimensional frequencies for single-fold laminated composite folded plates with 2-point and 3-point integration of mass matrices

Modes	E-glass–Epoxy folded plate with $\alpha = 90°$				E-glass–Epoxy folded plate with $\alpha = 120°$			
	$[30°/-30°]_S$		$[30°/-30°]_2$		$[30°/-30°]_S$		$[30°/-30°]_2$	
	Gauss points		Gauss points		Gauss points		Gauss points	
	2×2	3×3	2×2	3×3	2×2	3×3	2×2	3×3
1	0.0394	0.0394	0.0397	0.0397	0.0394	0.0394	0.0398	0.0398
2	0.0719	0.0718	0.0724	0.0723	0.0703	0.0703	0.0707	0.0707
3	0.1488	0.1483	0.1496	0.1491	0.1488	0.1483	0.1497	0.1492

time step Δt. The responses are observed to be more pronounced, as expected, with increasing fibre angle.

Example 5. In Fig. 8 the effect of number of plies is illustrated for single-fold E-glass–Epoxy composite, cantilever folded plates with crank angle $\alpha = 120°$. The data used are the same as those in Example 4. The two-ply and four-ply laminates show slight change in response in the second cycle, but the four-ply symmetric and anti-symmetric laminates have produced practically identical results. The six-ply anti-symmetric laminate has been observed to behave identically with the four-ply laminates.

Example 6. In Fig. 9 the effect of the crank angle is illustrated for two fold E-glass–Epoxy composite, cantilever folded plates with crank angles 90°, 120°, and 150°. The data used are the same as those in Example 4. The 90° cranked plate shows stiffest behaviour and quickly approaches to attain the state of static de-

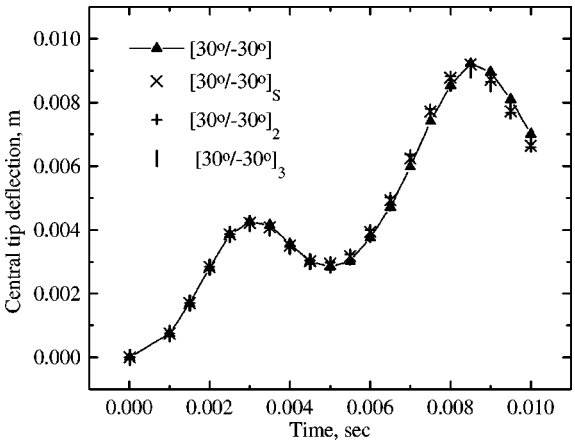

Fig. 8. Central tip deflection versus time for a cantilever single-fold folded plate with crank angle $\alpha = 120^\circ$, subjected to suddenly applied pulse loading (4×3 mesh).

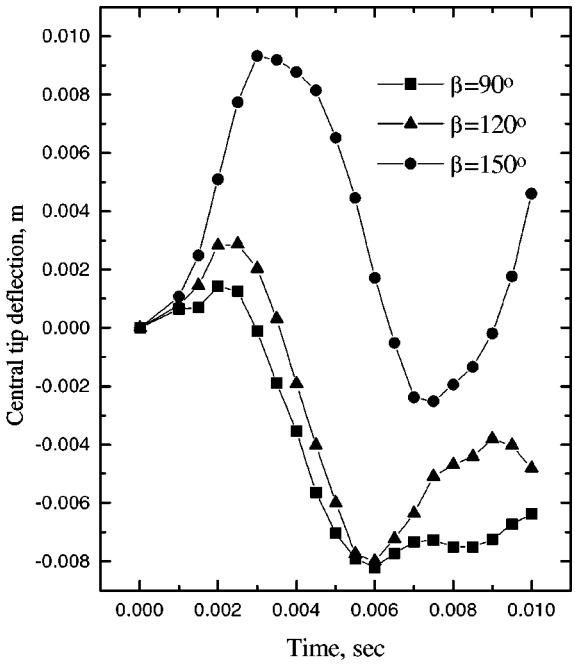

Fig. 9. Comparative study of central tip deflection for E-glass–Epoxy 2 fold laminated cantilever folded plates, with $30^\circ/-30^\circ$ lamination, 6×3 mesh.

flection, while the 150° cranked plate has the largest response and manifests most pronounced oscillation.

4. Conclusion

This paper is concerned with the dynamic analysis of laminated composite cantilever folded plate structures. For the numerical simulation of the problem finite element technique has been used. Various folded plate configurations have been considered in the present study. The results obtained from the present formulation for isotropic folded plate structure are compared with the semi-analytical solutions and finite element results available in the open literature and a good agreement is observed. A set of new results for laminated composite cantilever folded plate structures with various lamination schemes, crank angles, and stacking sequence are presented. Certain differences in free vibration modes of isotropic and composite folded plates have been highlighted. The first order shear deformation theory is found to work well for folded plates where the five regular degrees of freedom is appended with a sixth drilling degree of freedom as suggested in Zienkiewicz [21] and Bathe [1].

References

[1] K.J. Bathe, *Finite Element Procedures in Engineering Analysis*, Prentice Hall, Englewood Cliffs, 1982.

[2] C.W. Bert and T.L.C. Chen, Effect of shear deformation on vibration of antisymmetric angle-ply laminated rectangular plates, *Int. J. of Solids and Structures* **14** (1978), 465–473.

[3] S.N. Chatterjee and S.V. Kulkarni, Shear correction factors for laminated plates, *AIAA Journal* **17**(5) (1979), 498–499.

[4] A.N. Danial, Inverse solutions on folded plate structures, Ph.D. Dissertation, Purdue University, 1994.

[5] A.N. Danial, J.F. Doyle and S.A. Rizzi, Dynamic analysis of folded plate structures, *J. of Vibration and Acoustics*, Trans. ASME **118** (1996), 591–598.

[6] S.B. Dong and C.K. Chun, Shear constitutive relations for laminated anisotropic shells and plates: Part I – Methodology, *J. of Applied Mechanics* **59**(2) (1992), 372–379.

[7] A.L. Eterovic and L.A. Godoy, An exact-strip method for folded plate structures, *Computers and Structures* **32**(2) (1989), 263–276.

[8] J.E. Goldberg and H.L. Leve, Theory of prismatic folded plate structures, *Int. Association for Bridge and Structural Engineering J.* **17** (1957).

[9] B.W. Golley and W.A. Grice, Prismatic folded plate analysis using finite strip-elements, *Computer Methods in Applied Mechanics and Engineering* **76** (1989), 101–118.

[10] T. Irie, G. Yamada and Y. Kobayashi, Free vibration of a cantilever folded plate, *J. of the Acoustical Society of America* **76**(6) (1984), 1743–1748.

[11] T. Kant, J.H. Varaiya and C.P. Arora, Finite element transient analysis of composite and sandwich plates based on a refined theory and implicit time integration schemes, *Computers and Structures* **36**(3)(1990), 401–420.

[12] W.H. Liu and C.C. Huang, Vibration analysis of folded plates, *J. of Sound and Vibration* **157**(1)(1992), 123–137.

[13] D.K. Maiti and P.K. Sinha, Impact behaviour of thick laminated composite beams, *J. of Reinforced Plastics and Composites* **14**(3) (1995), 255–279.

[14] D.K. Maiti and P.K. Sinha, Bending, free vibration and impact response of thick laminated composite plates, *Computers and Structures* **59**(1) (1996), 115–129.

[15] D.K. Maiti and P.K. Sinha, Impact response of doubly curved laminated composite shells using higher-order shear deformation theories, *J. of Reinforced Plastics and Composites* **15** (6) (1996), 575–601.

[16] C. Meimaris and J.D. Day, Dynamic response of laminated anisotropic plates, *Computers and Structures* **55**(2) (1995), 269–278.

[17] M. Ohga and T. Shigematsu, Bending analysis of plates with variable thickness by boundary element-transfer matrix method, *Computers and Structures* **28**(5) (1987), 635–640.

[18] J.N. Reddy, A simple higher-order theory for laminated composite plates, *J. of Applied Mechanics* **51** (1984), 745–752.

[19] R. Suresh and S.K. Malhotra, Vibration and damping analysis of thin-walled box beams, *J. of Sound and Vibration* **215** (2) (1998), 201–210.

[20] T.Y. Tsui and P. Tong, Stability of transient solution of moderately thick plates by finite difference methods, *AIAA Journal* **3** (1971), 1772–1773.

[21] O.C. Zienkiewicz and R.L. Taylor, *The Finite Element Method*, Vol. 2, 4th edn, McGraw-Hill, 1991.